The time-dependent process of oxidation of the surface of Bi_2Te_3 studied by x-ray photoelectron spectroscopy

2000 J. Phys.: Condens. Matter 12 5607

(http://iopscience.iop.org/0953-8984/12/26/307)

J. Phys.: Condens. Matter **12** (2000) 5607–5616. Printed in the UK PII: S0953-8984(00)08687-2

The time-dependent process of oxidation of the surface of Bi_2Te_3 studied by x-ray photoelectron spectroscopy

H Bando†, K Koizumi†, Y Oikawa†, K Daikohara†, V A Kulbachinskii‡ and H Ozaki†

† Department of Electrical, Electronics and Computer Engineering, Waseda University, Ohkubo 3-4-1, Shinjuku-ku, Tokyo, 169-8555, Japan

‡ Low Temperature Physics Department, Moscow State University, 119899, Moscow, Russia

Received 13 October 1999, in final form 2 May 2000

Abstract. The process of oxidation of the Bi_2Te_3 surface was investigated by x-ray photoelectron spectroscopy (XPS). The oxidized surface layer was found to have a definite thickness, with configurations where O is bonded with Bi and Te, and Bi and Te are bonded with three and four oxygens, respectively. The oxidation time dependence of the oxidized layer thickness $d(t)$ estimated from the XPS behaved as $\sqrt{t - t_0}$ when $d(t)$ was smaller than the thickness of a single oxidized quintuple atomic layer in our oxide model and behaved as $t - t_1$ when it was larger than that. Experimental data were compared to our oxidation process model for the layered structure with the van der Waals gap and very good agreement was found.

1. Introduction

The bismuth telluride Bi_2Te_3 is known for its large thermoelectric figure of merit around room temperature and, at present, is most used as a Peltier device material. Bi_2Te_3 belongs to the class of layer semiconductors with the D^5_{3d} symmetry group. The crystal structure of Bi_2Te_3 consists of five atomic planes in the sequence Te(1)–Bi–Te(2)–Bi–Te(1), where Te(1) and Bi occupy the octahedral sites in the tetradymite structure (figure 1). The quintuple layers are stacked under the influence of the van der Waals force. The electronic structure of Bi_2Te_3 has been investigated by, e.g., x-ray photoelectron spectroscopy (XPS) [1–3] and synchrotron-radiation photoemission experiments [4], and by means of calculations [5, 6].

The Bi_2Te_3 crystal is easily cleaved along the van der Waals gap. This feature is useful for measurements requiring access to a fresh and flat surface such as tunnelling and XPS ones. Among the many layered structure materials, graphite and the transition metal dichalcogenides such as TaS_2 and MoS_2 are particularly well known for their stable flat surfaces when cleaved along the van der Waals gap. They have been observed using scanning tunnelling microscopy (STM) in the atmosphere at room temperature, and a clear image of the atomic arrays was obtained [7]. Similarly, the cleaved surface of Bi_2Te_3 has been generally considered to be stable and not to be oxidized in the atmosphere at room temperature, without a systematic investigation on the surface oxidation. However, when we tried to observe the cleaved surface of Bi_2Te_3 by STM, we found that, contrary to the case for graphite and 1T-TaS_2, the atomic STM image began to be blurred in one day after cleaving the surface (figure 2).

In the present work, we have carried out systematic measurements of the time-dependent process of oxidation of freshly cleaved surfaces of Bi_2Te_3 single crystals by XPS, and the results are explained by the proposed model of the oxidation process in this material.

0953-8984/00/265607+10$30.00

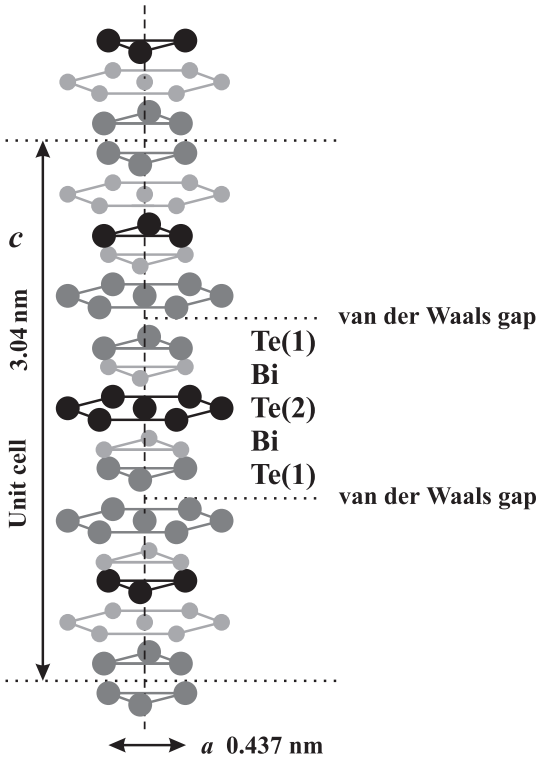

Figure 1. The crystal structure of Bi_2Te_3.

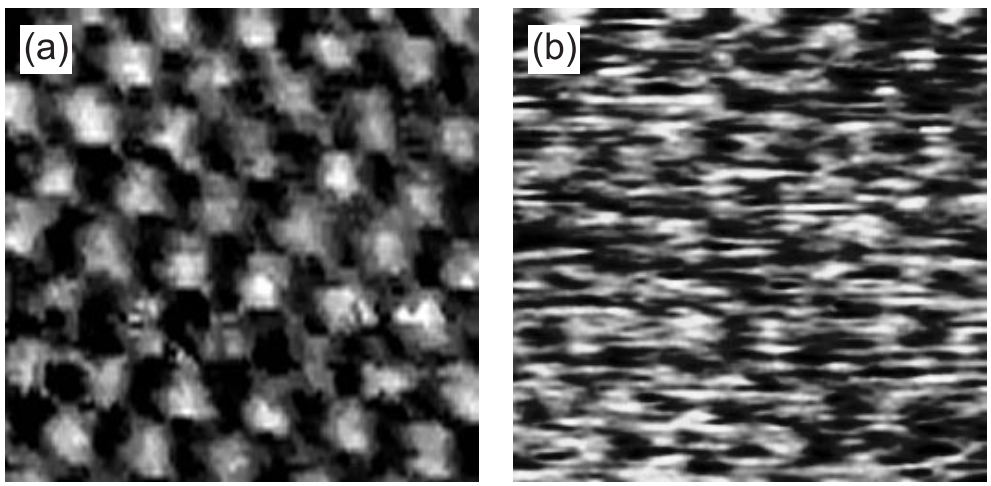

Figure 2. STM images of a 3×3 nm^2 Bi_2Te_3 surface in the atmosphere. $V_{tip} = 500$ mV. (a) Just after cleaving the surface. (b) 24 hours after cleaving.

2. Experimental procedure

Single crystals of Bi_2Te_3 were grown by the Bridgman method from polycrystalline materials. The starting polycrystalline materials were synthesized from 5N-purity elements mixed at the stoichiometric ratio in conical quartz ampoules. The Bi_2Te_3 grown always showed a p-type

conductivity. The typical value of the Hall coefficient at room temperature for the samples investigated was 1–2 $cm^3\ ^\circ C^{-1}$. The crystals can be easily cleaved perpendicular to the trigonal C_3-axis, i.e. along the (0001) plane.

Samples for measurements were first cut by a spark erosion machine into parallelepiped shapes (typically $4 \times 4 \times 1\ mm^3$). The surfaces were then cleaved with the help of adhesive tape in the atmosphere. Immediately after the cleaving, the samples were put into a desiccator box for oxidization, in which the humidity was controlled at 30% and the temperature at 24 °C. After a certain number of hours of this oxidization process, XPS measurements were performed on these samples at $(1–5) \times 10^{-7}$ Pa and at room temperature. After the XPS measurements, the samples were kept again under the conditions described above for various numbers of hours until the next XPS measurement was performed. This routine of oxidization and XPS measurements was carried out for up to 5700 hours for several samples. The XPS measurements were performed with a JEOL JPS-90 using Mg Kα ($\hbar\omega = 1253.6$ eV) radiation at the pass energy of 10 eV. The take-off angles ϕ of 0° and 60° relative to the normal of the sample surface were chosen in order to obtain information about the oxidation profile in the depth direction. The peak positions (binding energies) were calibrated using the Ag $3d_{5/2}$ peak (368.3 eV). The background was subtracted from the XPS spectra by the Shirley method [8,9]. The XPS spectra were decomposed into several Gaussian–Lorentzian peaks. The areas of the decomposed peaks were used as the intensities for the calculations in the following section. Though the intensities of Bi $4f_{7/2}$ and Te $3d_{5/2}$ are stronger than those of Bi $4f_{5/2}$ and Te $3d_{3/2}$, respectively, we used the latter in the analysis in order to avoid the influence of the satellite peaks of Bi $4f_{5/2}$ and Te $3d_{3/2}$, which came from the satellite x-ray Mg K$\alpha_{3,4}$, on the peaks of Bi $4f_{7/2}$ and Te $3d_{5/2}$, respectively.

3. Results

Figure 3 shows a series of Bi 4f and Te 3d XPS spectra for $\phi = 0°$ and 60° for one Bi_2Te_3 sample. The series of XPS spectra for other samples showed similar time-dependent behaviour.

The C 1s peak was observed at the binding energy 284.5 eV as shown in figure 4. This peak was usually observed in the XPS measurements when the sample surface was exposed to the atmosphere, and was attributed to a surface contamination. The intensity of this C 1s peak, which developed appreciably during the long oxidation time, did not increase so much as to decrease the intensities of the Bi 4f and the Te 3d spectra appreciably during the oxidation time. That is, the amount of carbon was below the level that would influence the XPS spectra of Bi_2Te_3. At zero oxidation time (when the sample was set in the XPS vacuum chamber just after the cleaving), there are only two peaks of Bi $4f_{7/2}$ and Bi $4f_{5/2}$ for the Bi 4f spectra and two peaks of Te $3d_{5/2}$ and Te $3d_{3/2}$ for the Te 3d spectra in Bi_2Te_3, without any peak for an oxide, for both $\phi = 0°$ and 60°. As the oxidation time increased, new peaks with one type of chemical shift grew in the Bi 4f and Te 3d spectra. We checked that the oxidation did not proceed during the XPS measurements, but it did during the time in which the sample was kept in the atmosphere. The intensities for $\phi = 60°$ for both Bi 4f and Te 3d spectra of the oxidized layer are remarkably strong compared to those for $\phi = 0°$ throughout the oxidation time. This shows that the depth of the oxidized layer is restricted to a few quintuple layers throughout the measured oxidation time.

Figure 5 shows the O 1s XPS spectra measured at oxidation times of 0, 24 and 280 hours for the Bi_2Te_3 surface. As shown in figure 5, just one peak with binding energy 529.9 eV grew with increasing oxidation time. The fact that the O 1s peak which grows with increasing oxidation time is the only one indicates that the nearest neighbours of O atoms are of one kind. Its binding energy lies between those for Bi_2O_3 and TeO_2. These binding energies are listed in

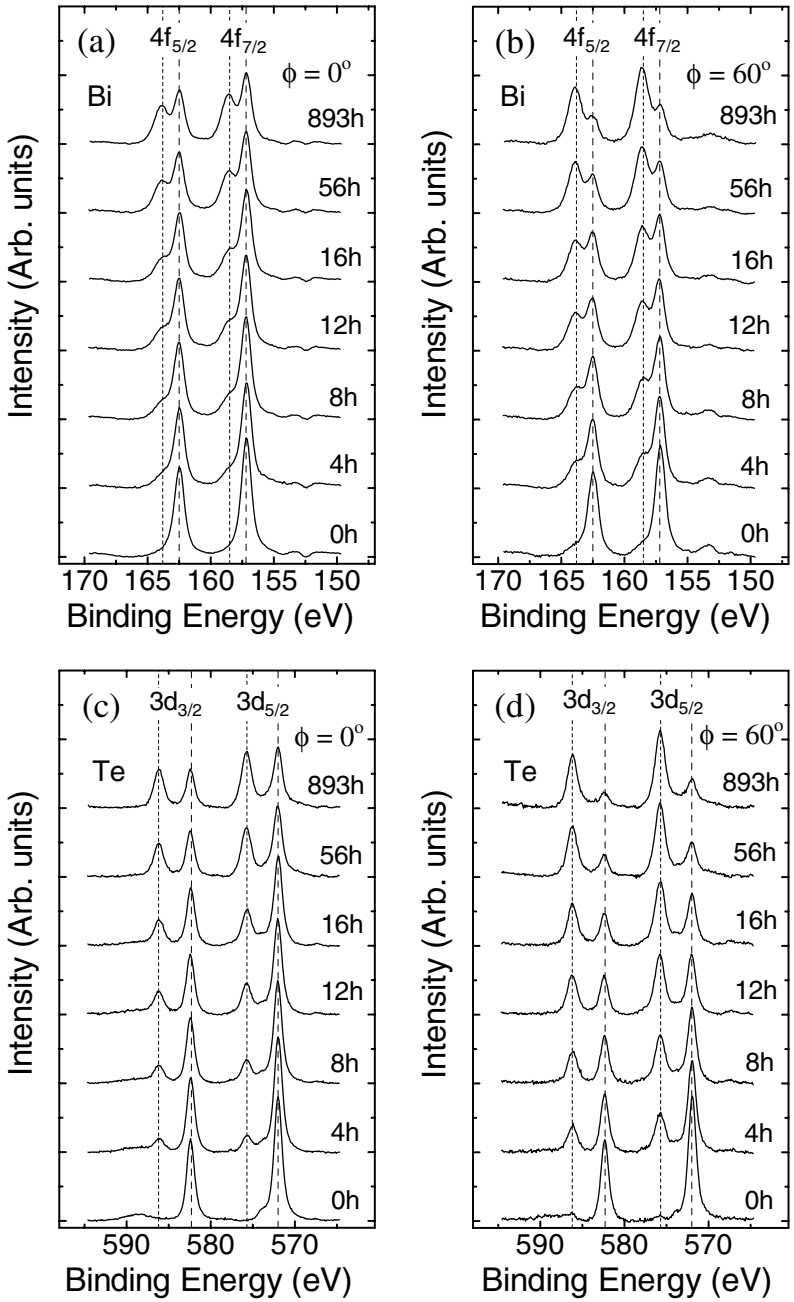

Figure 3. One set of Bi 4f and Te 3d XPS spectra for $\phi = 0^\circ$ and 60° for one Bi_2Te_3 sample. The oxidation was in the atmosphere, with humidity 30% and temperature 24 °C, for a series of oxidation times: 0 (just cleaved), 4, 8, 12, 16, 56 and 893 h.

table 1. Table 1 indicates that the oxidized states of a Bi and a Te atom in the oxidized surface are almost the same as those of Bi_2O_3 and TeO_2, respectively. These results indicate that each O atom forms a Bi–O–Te configuration.

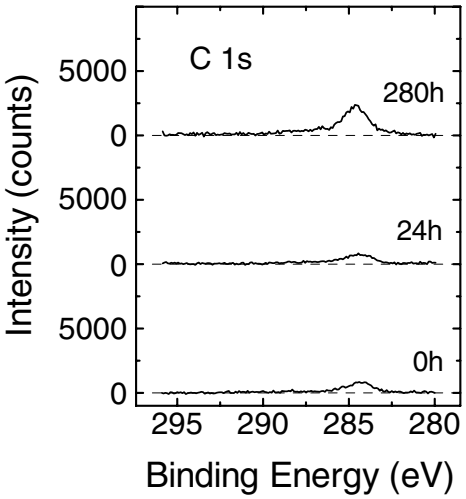

Figure 4. The C 1s XPS spectra for the Bi_2Te_3 surface for $\phi = 0^\circ$ measured at oxidation times of 0, 24 and 280 h.

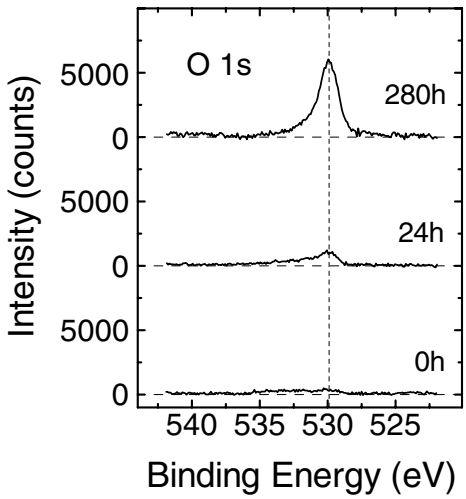

Figure 5. The O 1s XPS spectra for the Bi_2Te_3 surface for $\phi = 0^\circ$ measured at oxidation times of 0, 24 and 280 h.

Table 1. Binding energies in eV observed by XPS.

	Bi_2Te_3	Oxidized layer	Bi_2O_3 [1]	TeO_2 [10]
Bi $4f_{7/2}$	157.2	158.5	158.5	—
Bi $4f_{5/2}$	162.5	163.8	—	—
Te $3d_{5/2}$	572.0	575.7	—	575.9
Te $3d_{3/2}$	582.3	586.2	—	—
O 1s	—	529.9	529.1	530.2

4. Discussion

In view of the above results, we assume that the surface of Bi_2Te_3 has an oxidized layer with a definite thickness in which each Bi atom is bonded with O atoms, each Te atom is bonded with O atoms and each O atom is bonded with Bi and Te atoms. It is thus considered that the oxidized layer has the atomic configuration shown in figure 6(b). These structures are connected to each other to form an amorphous structure. In this model, the chemical environments around Bi and Te atoms in the oxidized layer are similar to those in crystalline Bi_2O_3 and TeO_2, respectively, within the first-nearest-neighbour region. Though it is possible that defect states such as –O–O– and dangling bonds exist in the amorphous structure, they are neglected in the present model used in the estimation of the oxidation layer thickness, because the XPS spectra show that their concentrations are low.

With the model shown in figure 6, we can estimate the thickness d of the oxidized layer from the XPS intensities and the take-off angle ϕ by using the following equation [11]:

$$d = \lambda^{\mathrm{oxide}} \cos\phi \ln\left[\alpha \frac{\lambda^{\mathrm{Bi_2Te_3}}}{\lambda^{\mathrm{oxide}}} \frac{I^{\mathrm{oxide}}}{I^{\mathrm{Bi_2Te_3}}} + 1\right] \tag{1}$$

where $I^{\mathrm{Bi_2Te_3}}$ and I^{oxide} are the intensities (i.e. peak areas) of the photoelectron peak of the Bi_2Te_3 and of the oxidized layer, respectively; $\lambda^{\mathrm{Bi_2Te_3}}$ and λ^{oxide} are the inelastic mean free

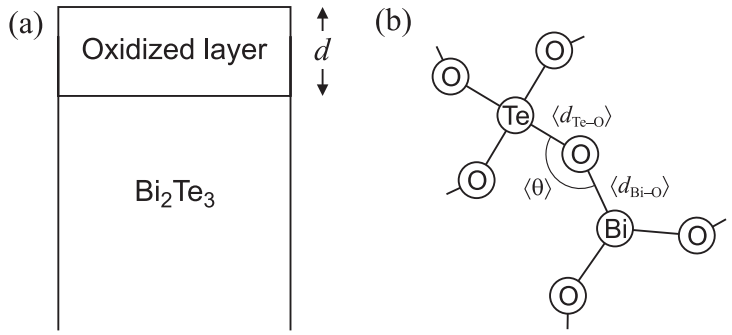

Figure 6. The model of the oxidized surface layer of Bi_2Te_3 based on the XPS results. (a) The oxidized surface layer of thickness d with amorphous structure. (b) The model assumed for the atomic configuration in the oxidized layer. The interatomic distances and the bond angle of oxygen are estimated by averaging the values for the respective crystals as $\langle d_{Bi-O}\rangle \approx 0.22$ nm, $\langle d_{Te-O}\rangle \approx 0.20$ nm and $\langle\theta\rangle \approx 150^\circ$.

paths (IMFPs) of the photoelectrons in the Bi_2Te_3 and the oxidized layer, respectively; α is the ratio of the volume density of the Bi or Te atoms in the Bi_2Te_3 to those in the oxidized layer. The values of the IMFPs were approximated, by using the TPP-2M [12] equations, to be 2.36 nm for Bi $4f_{5/2}$ peaks both in the Bi_2Te_3 and in the oxidized layer, and 1.65 and 1.67 nm for Te $3d_{3/2}$ peaks in the Bi_2Te_3 and in the oxidized layer, respectively. Though the value of α should be determined by further experiments, we estimated it to be $\approx$1.3 using an average Bi–O bond length of $\approx$0.22 nm for Bi_2O_3 [13] and an average Te–O bond length of $\approx$0.20 nm for TeO_2 [14], and taking the Bi–O–Te bond angle to be $\approx 150^\circ$ [13,14]. By using these values, the thickness of a single oxidized quintuple layer is estimated to be $\sim$1.1 nm.

Figure 7 shows the oxidation time dependence of the oxidized layer thickness estimated from the Te 3d spectra using equation (1) for several samples, where figure 7(b) shows the part

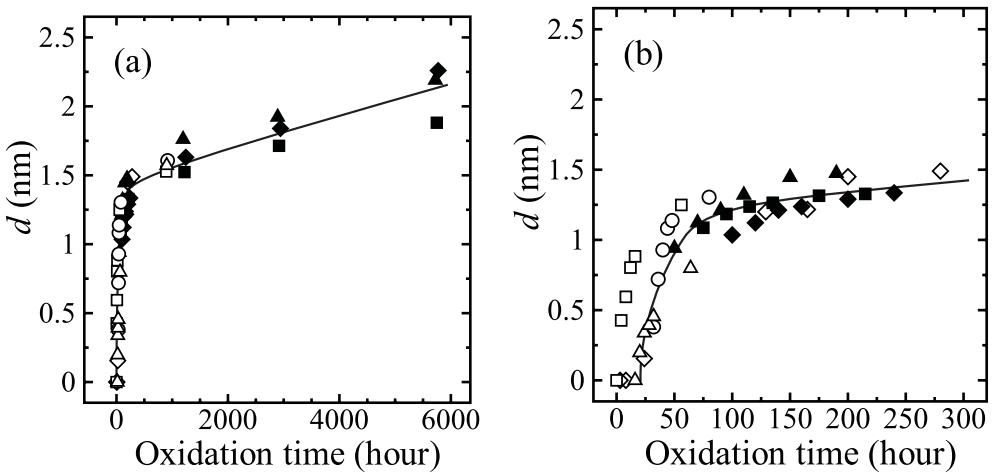

Figure 7. The oxidation time dependence of the oxidized layer thickness d on a Bi_2Te_3 surface derived from the Te 3d XPS spectra. Each set of symbols, except the ◇, denotes an oxidation series for one sample. (a) Oxidation time range 0–5800 h. (b) The part representing the first 0–300 h from (a).

representing the first 300 hours from figure 7(a) on an expanded scale. In figures 7(a) and 7(b), plots with a particular symbol denote an oxidation series for one sample, except that each ◊ denotes measurements for different samples.

The thicknesses similarly estimated from the Bi 4f spectra were about 1.1 times those estimated from the Te 3d spectra. The difference in the estimated thickness is due to the uncertainty in the approximated IMFPs. The discrepancy between the oxidized layer thicknesses calculated for $\phi = 0^\circ$ and for 60° was within the size of the symbols in figure 7 for the results from both Te 3d and Bi 4f spectra. This agreement shows that the present model is an appropriate one.

All series showed the behaviour $d \propto \sqrt{t - t_0}$ during the period when the value of the oxidized layer thickness d was less than ∼1.1 nm, and they increased more and more slowly with further increase in the oxidation time when the values of d exceeded ∼1.1 nm (see figures 7(b) and 8). Figure 7(b) shows that, except for one sample, there is an incubation time of ∼20 h before the oxidation starts.

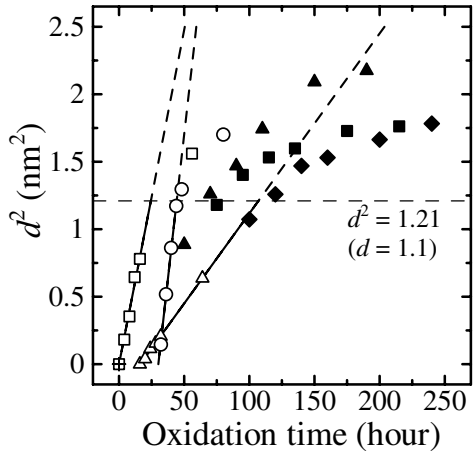

Figure 8. The square of the oxidized layer thickness (d^2) versus oxidation time.

We can explain the oxidation time dependence of the oxidized layer thickness using the following model.

(i) Process I: surface reaction. When the Bi_2Te_3 crystal is cleaved along the van der Waals gap, the Te(1) atoms on the cleaved surface are exposed to the atmosphere. In these circumstances, one important surface reaction is often the water-catalysed formation of carbonates originating from the reaction with atmospheric CO_2. In order to check on this possibility, the C 1s XPS measurements were performed for $\phi = 0^\circ$ and the spectra obtained are shown in figure 4. The dominant peak at 284.5 eV that originates from the adsorbed carbon on the surface is often used as the reference for the binding energy. The C 1s binding energies originating from carbonates distribute over 289–290 eV. Though the C 1s signal observed for longer oxidation time (280 h) extends its tail toward 290 eV, the fractional area of the 289–290 eV region is quite negligible. Thus, the concentration of carbonates in the oxidized layer is indicated to be negligible. The incubation time of the oxidation observed in figure 7(b) is connected with the initial surface reaction, and further investigations are needed if we are to understand its mechanism.

(ii) Process II. Once the surface is oxidized, O_2 molecules in the atmosphere enter the oxidized layer and diffuse through it. Though crystalline Bi_2Te_3 consists of quintuple atomic

layers, the oxidized layer is probably amorphous. Thus, we can treat the motion of the O_2 molecules in the oxidized layer as a continuous one, and describe it by the diffusion equation. When an O_2 molecule reaches the oxide/Bi_2Te_3 interface, it oxidizes the Bi_2Te_3 at the interface and thus the oxidized layer thickness increases. This oxidation process continues until the first quintuple layer of the Bi_2Te_3 surface is oxidized completely.

(iii) Process III. When the first quintuple layer of Bi_2Te_3 is oxidized completely ($d = d_1$), the O_2 molecule at the end of the first quintuple layer jumps to the second one over the van der Waals gap. In the second quintuple layer, the O_2 molecule oxidizes the Bi_2Te_3 by the same process as in the first quintuple layer. However, the oxidation in the second quintuple layer may not be so uniform as that in the first one, because the O_2 molecules arrive at the end of the first oxidized quintuple layer randomly by diffusing through it and, moreover, the frequency of jumping over the van der Waals gap is very low. The jumping process of the O_2 molecule perhaps occurs via intercalation sites in the van der Waals gap rather than as direct jumps from the first quintuple layer to the second one. These oxidation processes will proceed across the successive quintuple layers. However, the oxidized layer thickness looks likely to attain a saturation for a long oxidation time, because an O_2 molecule must jump over the van der Waals gap several times and this takes a very long time.

Process II, illustrated in figure 9(a), is expressed by the following equations [15, 16]:

$$\frac{\mathrm{d}x_{\mathrm{ox}}(t)}{\mathrm{d}t} = \frac{F_2}{C_1} \qquad (x_{\mathrm{ox}}(t_{\mathrm{i}}) = d_{\mathrm{i}}) \tag{2}$$

$$\frac{\partial C(x,t)}{\partial t} = D\frac{\partial^2 C(x,t)}{\partial x^2} \tag{3}$$

$$F_1 = -D\frac{\partial C(x,t)}{\partial x} \tag{4}$$

$$F_2 = kC(x_{\mathrm{ox}}, t) \tag{5}$$

where: $x_{\mathrm{ox}}(t)$ and $C(x,t)$ ($x > 0$, $t > t_{\mathrm{i}}$) are the oxidized layer thickness and the concentration of O_2 molecules in the oxidized layer, respectively; t_{i} and d_{i} are the initial time and the initial oxidized layer thickness, respectively; F_1 and F_2 are the fluxes of the O_2 molecules in the oxidized layer and at the oxide/Bi_2Te_3 interface, respectively; D is the diffusion coefficient of the O_2 molecules; k is the surface reaction rate constant at the oxide/Bi_2Te_3 interface; C_1 is the number of O_2 molecules in unit volume of the oxide. In the case of a steady state of oxidation—that is, when $F_1 = F_2$—equation (4) is expressed as $F_1 \simeq D[C_0 - C(x_{\mathrm{ox}}, t)]/x_{\mathrm{ox}}$, where C_0 is the surface concentration of O_2 molecules, which depends on the pressure of the O_2 molecules in the atmosphere for the first quintuple layer. In this case, one finds that

$$\frac{\mathrm{d}x_{\mathrm{ox}}}{\mathrm{d}t} = \frac{DC_0/C_1}{x_{\mathrm{ox}} + (D/k)} \tag{6}$$

and thus

$$x_{\mathrm{ox}}^2 + Ax_{\mathrm{ox}} = B(t - \tau) \tag{7}$$

where $A \equiv 2D/k$, $B \equiv 2DC_0/C_1$ and $\tau \equiv t_{\mathrm{i}} - (d_{\mathrm{i}}^2 + Ad_{\mathrm{i}})/B$. Equation (7) is solved by

$$x_{\mathrm{ox}}(t) = \frac{A}{2}\left[-1 + \sqrt{1 + \frac{4B}{A^2}(t - \tau)}\right]. \tag{8}$$

In process II ($x_{\mathrm{ox}}(t_0) = 0$—that is, $\tau = t_0$), the oxidized layer is very thin. In this case, the coefficient of diffusion in the oxidized layer is reduced by a compressive stress imposed by the Bi_2Te_3, and thus the value of A is fairly small [16]. Therefore, equation (7) can be

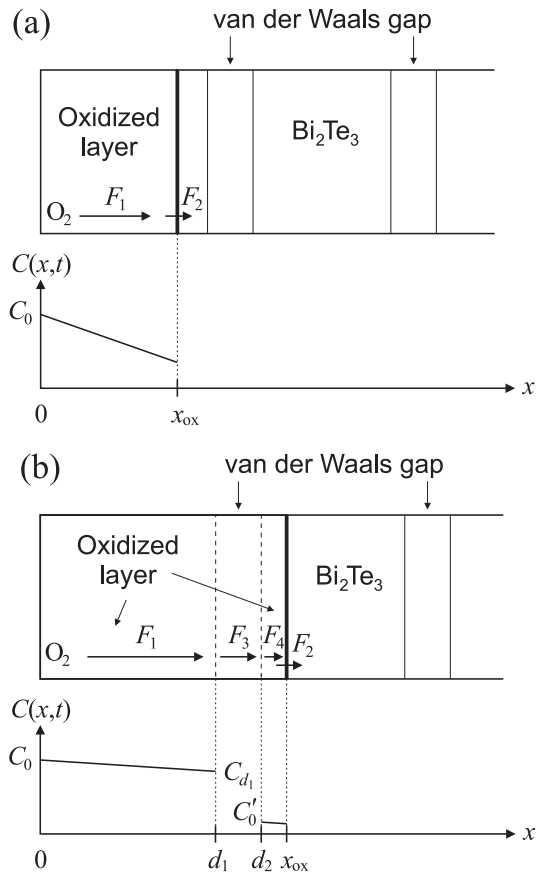

Figure 9. The oxidation process model. (a) Process II. (b) Process III.

approximated as $x_{ox}^2(t) \simeq B(t - t_0)$. This behaviour is observed experimentally, as seen in figure 8.

Process III, illustrated in figure 9(b), is expressed by equations (2)–(5) and the following equations:

$$F_3 = h[C(d_1, t) - C(d_2, t)] \tag{9}$$

$$F_4 = -D\frac{\partial C(x,t)}{\partial x} \tag{10}$$

where: h is the mass-transfer coefficient in the van der Waals gap; d_2 is the distance of the top of the second quintuple layer from the surface. In the steady state, $F_1 = F_2 = F_3 = F_4\ (=F)$, equations (4), (9) and (10) are expressed as $F_1 \simeq D[C_0 - C_{d_1}]$, $F_3 \simeq h[C_{d_1} - C'_0]$ and $F_4 \simeq D[C'_0 - C(x_{ox}, t)]$, respectively, where C_{d_1} and C'_0 are the concentrations of O_2 molecules at the bottom of the oxidized first quintuple layer and at the top of the second quintuple layer, respectively. Therefore, $x_{ox}(t)$ is expressed by the same form as equation (8) by replacing B with $B' \equiv 2DC'_0/C_1$ in process III. In process III ($x_{ox} > d_1$ for $t > t_1$), the source of O_2 molecules for the second quintuple layer is the oxidized first layer, separated from it by the van der Waals gap. The value of C_{d_1} is at most C_0 in the first oxidized layer. It is much smaller than that in the atmosphere. Furthermore, the jumping frequency of the O_2 molecule is very low. Therefore, C'_0 for the second quintuple layer is much smaller than C_0 for the first one.

Hence, B' is very small and equation (8) is written as $x_{ox}(t) \simeq B'(t-t_1)/A + d_1$ for the second quintuple layer. In this process, the flux F is very small and $C(x, t) \sim C_0$ in the first quintuple layer ($0 < x < d_1$). These behaviours of $x_{ox}(t)$ agree with our experimental results; that is, $x_{ox} \propto \sqrt{t - t_0}$ at the beginning of the oxidation time (in figure 8) and $x_{ox} \propto t - t_1$ for longer oxidation time as in figure 7(a).

5. Conclusions

The binding energies of Bi 4f, Te 3d and O 1s core electrons of Bi_2Te_3 surfaces were measured by XPS for $\phi = 0^\circ$ and 60° at various oxidation times up to 5700 hours. The oxidized layer thickness was estimated from the XPS results on the basis of our structure model for the oxidized layer. The oxidation time dependence of the oxidized layer thickness was explained very well by our oxidation process model for the layered structure with the van der Waals gap, in which the Deal–Grove diffusion model was applied to the oxidation process within the quintuple atomic layer of Bi_2Te_3.

References

[1] Debies T P and Rabalais J W 1977 *Chem. Phys.* **20** 277
[2] Chassé T and Berg U 1985 *Cryst. Res. Technol.* **20** 1475
[3] Scrocco M 1990 *J. Electron Spectrosc.* **50** 171
[4] Thuler M R, Benbow R L and Hurych Z 1982 *Chem. Phys.* **71** 265
[5] Pecheur P and Toussaint G 1989 *Phys. Lett.* A **135** 223
[6] Mishra S K, Satpathy S and Jepsen O 1997 *J. Phys.: Condens. Matter* **9** 461
[7] Wu X L, Zhou P and Lieber C M 1988 *Phys. Rev. Lett.* **61** 2604
[8] Shirley D A 1972 *Phys. Rev.* B **5** 4709
[9] Proctor A and Sherwood M A 1982 *Anal. Chem.* **54** 13
[10] Chowdari B V R and Kumari P P 1996 *J. Non-Cryst. Solids* **197** 31
[11] Strohmeier B R 1990 *Surf. Interface Anal.* **15** 51
[12] Tanuma S, Powell C J and Penn D R 1993 *Surf. Interface Anal.* **21** 165
[13] Harwig H A 1978 *Z. Anorg. Allg. Chem.* **444** 151
[14] Thomas P A 1988 *J. Phys. C: Solid State Phys.* **21** 4611
[15] Deal B E and Grove A S 1965 *J. Appl. Phys.* **36** 3770
[16] Sze S M 1985 *Semiconductor Devices Physics and Technology* (New York: Wiley) pp 342–51
[17] Horák J, Starý Z and Votinský J 1994 *Phil. Mag.* B **69** 31